



University of HUDDERSFIELD

University of Huddersfield Repository

Hamad, Naima, Brethee, Khaldoon F., Gu, Fengshou and Ball, Andrew

An Investigation of Electrical Motor Parameters in a Sensorless Variable Speed Drive for Machine Fault Diagnosis

Original Citation

Hamad, Naima, Brethee, Khaldoon F., Gu, Fengshou and Ball, Andrew (2016) An Investigation of Electrical Motor Parameters in a Sensorless Variable Speed Drive for Machine Fault Diagnosis. In: Proceedings 22nd International Conference on Automation and Computing (ICAC). IEEE. ISBN 9781862181328

This version is available at <http://eprints.hud.ac.uk/id/eprint/29511/>

The University Repository is a digital collection of the research output of the University, available on Open Access. Copyright and Moral Rights for the items on this site are retained by the individual author and/or other copyright owners. Users may access full items free of charge; copies of full text items generally can be reproduced, displayed or performed and given to third parties in any format or medium for personal research or study, educational or not-for-profit purposes without prior permission or charge, provided:

- The authors, title and full bibliographic details is credited in any copy;
- A hyperlink and/or URL is included for the original metadata page; and
- The content is not changed in any way.

For more information, including our policy and submission procedure, please contact the Repository Team at: E.mailbox@hud.ac.uk.

<http://eprints.hud.ac.uk/>

An Investigation of Electrical Motor Parameters in a Sensorless Variable Speed Drive for Machine Fault Diagnosis

Naima.Hamad^{1,2}, Khaldoon F. Brethee¹, Fengshou Gu¹ and Andrew D. Ball¹

¹Centre of Efficiency and Performance Engineering, University of Huddersfield, Queensgate, Huddersfield HD1 3DH, UK

²Department of Electrical Engineering, Omar Al-Mukhtar University, Albayda, Libya

E-mail: Naima.Hamad@hud.ac.uk

Abstract— Motor current signature analysis (MCSA) is regarded as an effective technique for motor and its downstream equipment fault diagnostics. However, limited work has been carried out for motors based on a sensorless variable speed drive (VSD). This study focuses on investigation of mechanical fault detection and diagnosis using electrical signatures from a VSD system. An analytic analysis was conducted to show that the fault can induce sidebands in instantaneous current, voltage and power signals in the VSD system, rather than just the sideband in a drive without closed loop control. Then different degrees of tooth breakages in an industrial two-stage helical gearbox were experimentally studied. It has found that even though the measured signal is very noisy, common spectrum analysis can discriminate the small sidebands for the fault detection and diagnosis. However, it has found that the power signals resulted from the multiplication of the current and voltage can provide a better diagnostic result.

Keywords- *electrical motor signature analysis; Sensorless variable speed drive; gearbox; tooth breakage.*

I. INTRODUCTION

Induction motors (IM) are the backbone of many industry applications due to their reliability and robustness. However, they are liable to different faults which may be induced by their operating environments. For safety reasons, an online fault diagnosis for induction machines is necessary in order to increase the reliability of the system and also prevent faults from progressing to high severity [1-3].

In IM, high performance is important to produce an efficient operation service. To do this, the IM must run with a small slip. Therefore, the most efficient strategy for speed control must be based on changing the synchronous speed rather than the slip. The supply frequency and the number of poles are the two main variables that determine the speed of the IM. The best method to adjust the speed over a wide range is to provide a variable-frequency supply; which can be implemented by the VSD [4]. When setting the VSD to a sensorless mode, certain variables will be adjusted, including speed, terminal voltages and stator currents. The regulation mechanism for speed responds is by compensating for any changes based on altered loads or

other factors. The drive changes the terminal voltage more than the current due to its attempt to keep speed constantly near to the desired level. Thus, more information about the motor conditions can be obtained by means of the voltage signals. It means that any mechanical problem such as tooth breakage will influence the current, voltage and power signals. Therefore, these signals can be used to diagnose gear tooth breakage [5-7].

MCSA has been found to be the most effective technique in fault diagnosis. It can utilize a clear indication to spot an existing or incipient failure using spectral analysis of the stator current of an induction motor. Moreover, MCSA is capable of detecting and analyzing the current components in terms of monitoring and diagnosis different faults such as broken rotor bars, air gap eccentricity, and shorted turns [3].

Connecting the IM through sensorless VSD allows control of the rotational speed to provide better dynamic response to any load changes, save energy and use power supply parameters to estimate speed and flux without sensors [8]. However, the closed-loop system induces a level of noise to the current and voltage measurements which masks some characteristics and prevents receipt of clear information [9, 10]. Little work has been found on the diagnosis performance of current, voltage and power signals with sensorless VSDs which are extensively used in industrial drives for their advantages.

In previous work [11], the diagnosis of motor stator faults for current and voltage signals under both open and closed-loop operation modes was discussed, hence the sensorless control gives more reliable and accurate diagnostic results. Moreover, MCSA method is used in [12] to detect the early onset of motor efficiency reduction in AC motors controlled by modern sensorless-vector variable speed control inverters. The dynamic response of the electrical current signals with a VSD for monitoring mechanical faults from a downstream gearbox using an open-loop control was investigated in [13]. Furthermore, the study in [14] provided the details for application of a modulation signal bispectrum analysis of current signals to enhance feature components for the detection of the stator faults using an open-loop control mode. A new scheme for sensorless Field Oriented Control with on-line speed and

rotor resistance using a new type of estimator for artificial neural networks to improve the induction motor driver performance and extend the induction motor lifetime was presented in [15]. In [7], the diagnosis of broken rotor bar based on sensorless VSD was investigated. It shows that components at twice slip frequency can be extracted more accurately in the power spectrum and also provide better results in separating different cases for broken rotor bar under sensorless VSD. However, review of the literature shows that in mechanical faults systems for example, tooth breakage, driven by a sensorless VSD are not well studied.

This work examines the capability of using electrical motor signatures driven by a sensorless VSD for monitoring and diagnostic of a mechanical system fault. Based on a two-stage helical gearbox transmission system, current, voltage and power signature analyses with small degrees of tooth breakage are investigated under different operating conditions.

II. ELECTRICAL MOTOR SIGNATURE ANALYSIS

A. Sensorless variable speed drive

In recent years, VSDs are increasingly turned within industrial spheres to give greater production efficiency. When setting the VSD to a mode without sensor action, certain variables will be altered, including speed, terminal voltages and stator currents. The regulation mechanism for speed responds to this by compensating for changes based on altered loads or other factors. The drive changes the terminal voltage more than the current due to its attempt to keep speed constantly near to the desired level. Thus, more information about the motor condition can be obtained by means of the voltage signals. On the other hand, the noise from the drive and the controlling activities of the closed loop hinder extraction of clarity data [5, 6].

A feedback loop is added in order to provide a better speed regulation and enhance the dynamic response. For sensorless VSD, there are many different schemes which are almost the same in basic structure. A typical type is shown in Fig. 1. [16]. For high performance reasons, systems for control frequently contain a number of control loops. The outermost is speed PI control loop, viewing speed measured values in comparison to reference figures, and producing the speed error which allows rising or lowering of outputs to match the set point. Variables of process are handled by the outer control loop, in which the speed regulator loop is within the process regulating loop and the torque regulator loop is the innermost loop. The inner control loop consists of two PI control loops [11, 17]:

- The current loop which compares between the estimated current and the reference to set the reference torque signal;
- The torque control loop which regulates the required voltage component based on the output of the current loop.

Another loop is the voltage control loop, which transfers the voltage component to the PWM. Finally, the field control loop which keeps the flux fixed at the rated speed in case if the speed is less than the base motor speed.

However, when the speed is at or higher than the rated speed, the flux will be lowered by using field weakening by $(1/\omega_r)$ where ω_r is the rotor angular frequency [11, 17, 18]. For stability purposes, the inner loop (torque loop) must be from three to ten times faster than the outer loop (current loop) and also the current loop should be three to ten times more than the speed loop. As represented in Fig. 1. [16], when a fault occurs, the speed will change and the drive will detect it, then the speed regulator will transfer a speed error to the speed control loop which will promote the torque control i_q .

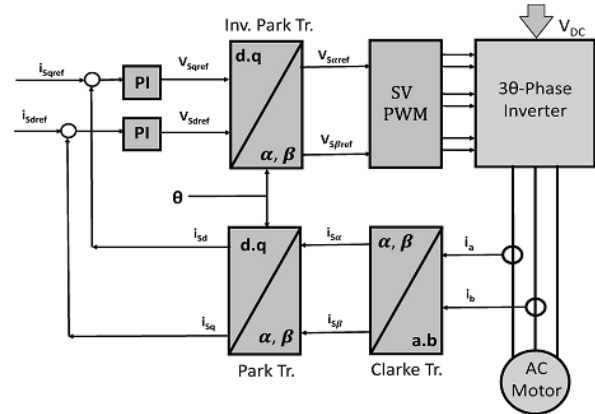


Figure 1. Sensorless vector control block diagram [15]

The output from the current controller sets the reference torque required so as to compensate any changes. Consequently, the torque controller will compare this reference torque with the estimated torque which outputs the desired torque voltage V_q to the PWM and then to the motor. Furthermore, the field current component i_d sets the desired flux Ψ which is kept constant at the rated speed when the speed is less than the base motor speed. However, in case of small faults, the noise caused by the drive and the control actions of the closed loop mask the features extracted in the current signal, hindering the detection of the current signal [16-18].

B. Effect of a fault on the electrical parameters

It is worth mentioning that mechanical abnormalities eventuate additional load oscillations around the electrical torque which are regulated at frequency f_F that is linked with the rotational frequency f_r and the supply frequency f_s [19, 20]. Based on the study in [19], the current signal in only one phase (A) for the motor in a healthy case is described by the following relationship:

$$i_A = \sqrt{2}I \cos(2\pi f_s t - \alpha_I) \quad (1)$$

Likewise, the flux of the stator can be written as:

$$\psi_A = \sqrt{2}\psi \cos(2\pi f_s t - \alpha_\psi) \quad (2)$$

As the torque can be generated by the interaction of the current flowing in the rotor bars and the air gap flux, thus, the expression of the torque will be as follows:

$$T_{em} = 3P\psi I \sin(\alpha_I - \alpha_\psi) \quad (3)$$

Where I and Ψ are the root mean square values of the supply current and air gap flux, α_I and α_ψ are the phases of the current and flux, f_s is the supply frequency and P is the number of pole pairs [16, 21]. Consequently, the additional torque caused by the fault is supposing to be a sinusoidal wave with a current of I_F , a phase of α_F and a frequency of f_F is expressed as the following:

$$\Delta T_{em} = 3P\psi I_F \sin(2\pi f_F t - (\alpha_I - \alpha_\psi) - \alpha_F) \quad (4)$$

The mechanical speed of the induction motor is represented as:

$$\frac{d\omega_r(t)}{dt} = \frac{1}{J} (T_{em}(t) - T_{load}(t)) \quad (5)$$

Because of the fault occurring, the speed of the motor (ω_r) will also oscillate by $\Delta\omega_r$ as indicated in the following equation:

$$\Delta\omega_r = \frac{P}{J} \int \Delta T_{em} dt = -\frac{3P^2\psi I_F}{2\pi f_F J} \cos(2\pi f_F t - (\alpha_I - \alpha_\psi) - \alpha_F) \quad (6)$$

Consequently, the angular variation in the rotor will be:

$$\Delta\alpha_F = \Delta\theta = \frac{P}{J} \int \Delta\omega dt = \frac{3P^2\psi I_F}{4\pi^2 f_F^2 J} \sin(2\pi f_F t - (\alpha_I - \alpha_\psi) - \alpha_F) \quad (7)$$

The oscillations in the load due to mechanical fault result in torque component that modulates the motor speed and causes speed fluctuations which in turn change the rotor position. Therefore, these fluctuations in the rotor position affect the slip frequency and consequently, the torque current component will be also affected by the fault. The angular fluctuation will modulate the flux as is given in the following equation:

$$\psi_A^F = \sqrt{2}\psi \cos[2\pi f_s t - \alpha_\psi - \Delta\psi \sin(2\pi f_F t - (\alpha_I - \alpha_\psi) - \alpha_F)] \quad (8)$$

$$\text{Where } \Delta\psi = \frac{3P^2\psi I_F}{4\pi^2 f_F^2 J}$$

$$\psi_A^F = \sqrt{2}\psi \cos(2\pi f_s t - \alpha_\psi) + \sqrt{2}\psi \Delta\alpha_F \sin(2\pi f_F t - \alpha_\psi) \quad (9)$$

$$\begin{aligned} \psi_A^F &= \sqrt{2}\psi \cos(2\pi f_s t - \alpha_\psi) \\ &+ \sqrt{2}\psi \Delta\psi \cos[2\pi(f_s - f_F)t - \alpha_I - \alpha_F] \\ &- \sqrt{2}\psi \Delta\psi \cos[2\pi(f_s + f_F)t - 2\alpha_\psi + \alpha_I - \alpha_F] \end{aligned} \quad (10)$$

It is noticeable that the flux in equation (10) contains two components; the fundamental frequency and also the sidebands around it [19]. Based on the analysis in [10, 22], the interaction between the stator flux and the equivalent circuit impedance produces sideband components around the supply frequency of the current and voltage signals as represented in the following relationships:

$$\begin{aligned} i_A^F(t) &= \sqrt{2}I \cos(2\pi f_s t - \alpha_I) \\ &+ \sqrt{2}I_l \cos[2\pi(f_s - f_F)t - \alpha_I - \alpha_F - \varphi] \\ &+ \sqrt{2}I_r \cos[2\pi(f_s + f_F)t - 2\alpha_\psi + \alpha_I - \alpha_F - \varphi] \end{aligned} \quad (11)$$

$$\begin{aligned} u^F(t) &= \sqrt{2}U \cos(2\pi f_s t) \\ &+ \sqrt{2}U_l \cos[2\pi(f_s - f_F)t - \alpha_F - \varphi] \\ &+ \sqrt{2}U_r \cos[2\pi(f_s + f_F)t - 2\alpha_\psi + \varphi_F - \varphi] \end{aligned} \quad (12)$$

Where φ is the angular displacement of motor equivalent circuit impedance at supply frequency, I_l , I_r , U_l and U_r are the RMS values of the lower and the upper sideband components of the current and voltage, respectively, at frequencies of $f_s - f_F$ and $f_s + f_F$, α_I is the phase angle between voltage and current, α_ψ is the phase angle between the stator flux and voltage, and f_F is the fault frequency. Equation (11) shows that the current signal for the faulty case demonstrates additional components compared to that for healthy case. The corresponding power in the case of the fault will be expressed in the following formula:

$$\begin{aligned} p^F(t) &= \frac{IU}{2} [1 + \cos(2\omega_s t)] \\ &+ \frac{IU_l}{2} [\cos(\omega_f t) + \cos(2\omega_s t - \omega_f t)] \\ &+ \frac{IU_r}{2} [\cos(-\omega_f t) + \cos(2\omega_s t + \omega_f t)] \\ &+ \frac{I_r U}{2} [\cos(-\omega_f t) + \cos(2\omega_s t + \omega_f t)] \\ &+ \frac{I_r U_r}{2} [1 + \cos(2\omega_s + 2\omega_f)t] \\ &+ \frac{I_r U_l}{2} [\cos(2\omega_f)t + \cos(2\omega_s)t] \\ &+ \frac{I_l U}{2} [\cos(-\omega_f)t + \cos(2\omega_s - \omega_f)t] \\ &+ \frac{I_l U_r}{2} [\cos(2\omega_s)t + \cos(-2\omega_f)t] \\ &+ \frac{I_l U_l}{2} [1 + \cos(2\omega_s - 2\omega_f)t] \end{aligned} \quad (13)$$

Where, $\omega_s = 2\pi f_s$, $\omega_f = 2\pi f_F$, ω_s is the angular supply frequency and ω_f is the angular fault frequency. For simplicity, the phase angles are excluded from the trigonometric equations in which the presented features are close to a real power signal. As a result, an effective analysis can be applied.

$$\begin{aligned}
p^F = & \frac{IU + I_r U_l + I_l U_r}{2} \cos(2\omega_s t) \\
& + \frac{I U_l + I U_r + I_r U + I_l U}{2} \cos(\omega_f t) \\
& + \frac{I_r U_l + I_l U_r}{2} \cos(2\omega_f t) \\
& + \frac{I U_l + I_l U}{2} \cos(2\omega_s - \omega_f) t \\
& + \frac{I U_r + I_r U}{2} \cos(2\omega_s + \omega_f) t \\
& + \frac{I_r U_r}{2} \cos(2\omega_s + 2\omega_f) t \\
& + \frac{I_l U_l}{2} \cos(2\omega_s - 2\omega_f) t
\end{aligned} \quad (14)$$

From equation (14), it can be seen that the power spectrum has more features frequency components than that in current and voltage. Due to the modulation effect, the first harmonic of the supply frequency is disappeared whereas the second harmonic ($2\omega_s$) is appeared alternately. Moreover, two sideband components appear at $2\omega_s \pm 2\omega_f$ in addition to another two sidebands at $2\omega_s \pm \omega_f$. The amplitude of these two sidebands will change with the load fluctuations and hence, the sidebands will be different from that of healthy motor [19]. The sideband components in each electrical parameter will stimulate the drive's regulators for the sake of maintaining the speed of the machine. However, such frequency components and also the small changes due to incipient faults may be obscured by the drive's noise and actions making the detection difficult, consequently, more advanced signal processing techniques need to be used [10, 19].

Based on the above discussion, when the motor driven by a sensorless VSD, the mechanical abnormalities cause additional load oscillations that are mostly regulated at frequency (f_F), which is related to the rotating speed (f_r) and the supply frequency. Load oscillations can be detected by the speed control loop if its frequency is within its bandwidth. In the case of PI controller, the i_{qs}^* and the i_{ds}^* components are calculated from the following equations [10]:

$$i_{qs}^* = (\omega_r^* - \omega_r + \Delta\omega_r)(k_p + \frac{k_i}{S}) \quad (15)$$

and the field current reference is produced by:

$$i_{ds}^* = (\psi_r^* - \psi_r + \Delta\psi_r)(k_p + \frac{k_i}{S}) \quad (16)$$

where k_p denotes the PI controller proportional gain, k_i is the PI controller integral gain and ψ_r is the rotor flux. The field and the speed controller are the outer loops whereas torque, current and voltage loops are the inner loops, which have wider range of bandwidth than that of the outer loops. Consequently, the current control loop can respond faster than the speed control loop and can detect faults at frequencies out of the speed loop bandwidth range.

However, the current loop bandwidth is limited by the voltage control loop bandwidth and not all the frequency ranges will pass through the current regulators [10].

III. TEST FACILITY AND PROCEDURE

Figure 2 shows the test facility used in this work which consists of a 15kW AC induction motor at 1460rpm (two-pole pairs), driven by a VSD. A back-to-back two-stage helical gearbox is driven by the IM and connected to a DC motor via flexible coupling, which acts as a mechanical load. The gear teeth numbers are 58/47 for the first stage and 13/59 for the second stage, with a total gear ratio of 3.678. The first gearbox (GB1) that connected to the induction motor acts as a speed reducer whereas the other is a speed increaser. The test rig is controlled by a Programmable Logic Control (PLC) which delivers the required test profile to both AC and DC VSDs. The AC drive, (Parker 650V) that adjusts the speed, can be set either to a V/Hz or a sensorless flux vector control mode. In sensorless mode, the drive estimates the system speed based on the Model Reference Adaptive system (MRAS). In this work, the VSD set under sensorless mode in order to evaluate its capability to detect mechanical fault in the system.

A high speed data acquisition system (YE6232B), 16 channels was used to record the data from different sensors with a sampling frequency of 96 kHz. Six sensors were used to record the electrical signals of three-phase currents and voltages. The collected data through the acquisition system is sent to a PC for processing and analyzing. An encoder is connected directly to the data acquisition system as a speed indicator. Then, all recorded data will be converted to a Matlab for analysis. Different tooth breakage severities (20% and 40% of the tooth width) under different operating conditions were carried out in GB1 in order to examine the capability of using electrical signatures analysis to diagnose small degrees of mechanical fault.

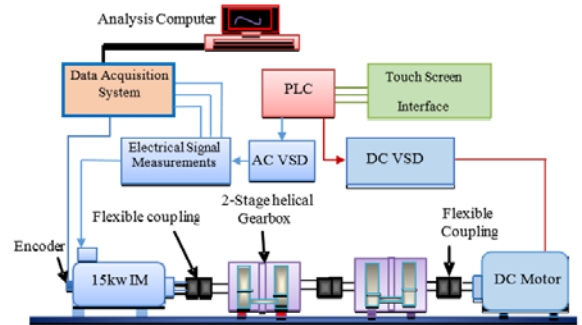


Figure 2. Mechanical part of the test rig

IV. RESULTS AND DISCUSSION

For identification and tracking of individual frequency components, electrical signal spectra are used to evaluate the physical machine characteristics. Figures 3, 4 and 5 represent the spectra of the current, voltage and power of healthy and faulty cases under different operating conditions. From the current spectrum (Fig. 3), it can be seen that the amplitude of the sidebands significantly increases as the load and fault severity increase.

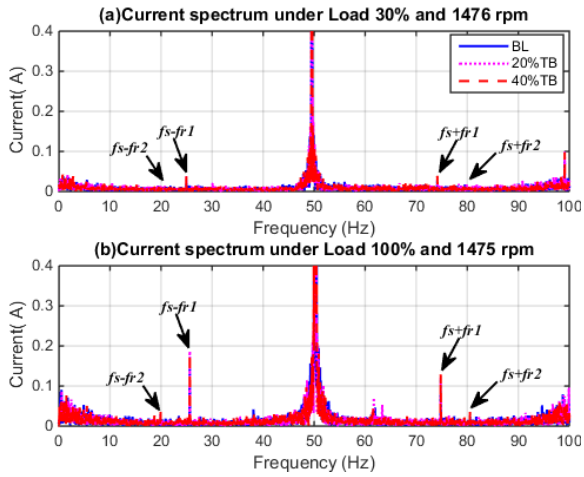


Figure 3. Current spectrum under different loads and full speed

Due to the fact that these components are related to the motor shaft frequency, it is believed that the appearance of these components is caused by the tooth defect. The gear tooth breakage on the gear causes more significant change of the dynamic components of f_{r2} . Figure 4 shows prominent increases in the upper and lower sidebands amplitude of the voltage spectrum, which also increase with load and the fault severity.

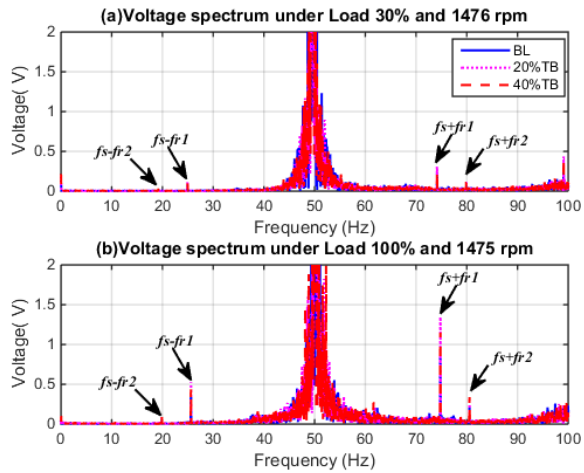


Figure 4. Voltage spectrum under different loads and full speed

Figure 5 depicts the power spectrum, in a similar way to the current and voltage spectra, the amplitude characteristics for the upper and the lower sideband components clearly appear and exhibit similar variations with the degree of the fault and under all load conditions. However, the power spectrum has a peak at $2f_s$ (100 Hz) as explained in equation (14). It is clear that the power spectrum has more frequency components than those for current and voltage. Furthermore, two sideband components appear at $2\omega_s \pm 2\omega_F$ in addition to another two sidebands at $2\omega_s \pm \omega_F$.

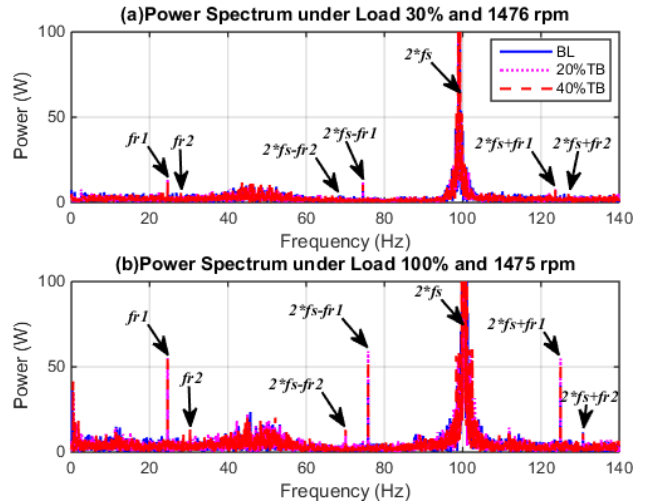


Figure 5. Power spectrum under different loads and full speed

Due to the fact that the sideband components are linked to the shaft frequencies, it should be noticed that the amplitude of the 20% tooth damage at f_{r2} at some points is higher than that of the 40%, which is due to the interaction between the tooth fault, misalignment, gear errors (from manufacturing and installation) and load variations. For more accurate data, the test set was repeated five times. The current amplitudes at upper and lower sideband frequency of the all tests are shown in Figure 6, which displays a noticeable difference between the three cases.

An increase in fault severity causes an increase in noise, which in turn will cause an overlap in the signals, and this affects detection. Furthermore, the current graph exhibits an inconsistent change in the amplitudes for the upper and the lower sideband components for the five tests in parallel with the increment in the load and also the severity of the fault from 20% of tooth breakage to 40%.

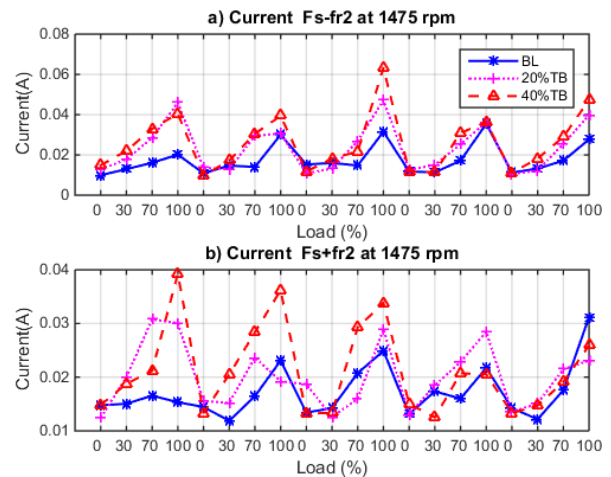


Figure 6. The current amplitudes at upper and lower sidebands frequency for the three cases

Similarly, the voltage amplitudes at upper and lower sidebands frequency are shown in Figure 7. The fault was introduced in the pinion gear of the first stage; therefore, the middle shaft frequency (f_{r2}) will be affected by the fault more than the input shaft frequency (f_{r1}). The voltage spectrum gives a considerable difference between the

cases. In particular, it provides more consistent change with the fault severity.

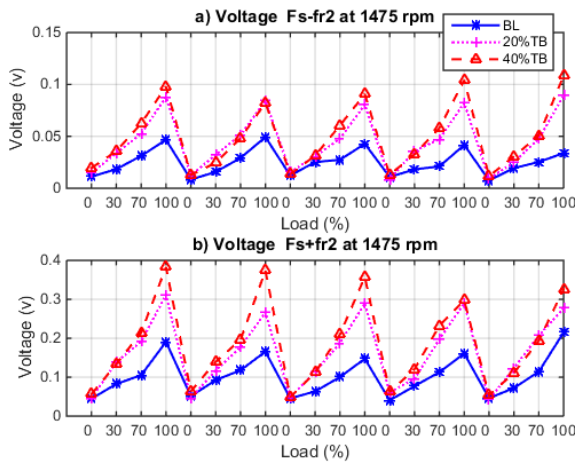


Figure 7. The voltage amplitudes at upper and lower sidebands frequency for the three cases

The following figures show the average peaks of the current, voltage and power at the lower and upper sidebands of f_{r2} . It can be seen that these features are enhanced clearly with the load and fault severity. However, more significant and consistent change is identified in the power spectrum.

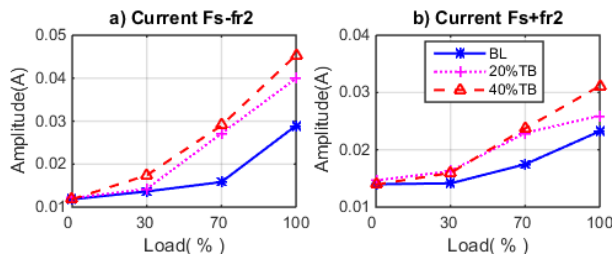


Figure 8. Current peaks at the lower and upper sidebands frequency

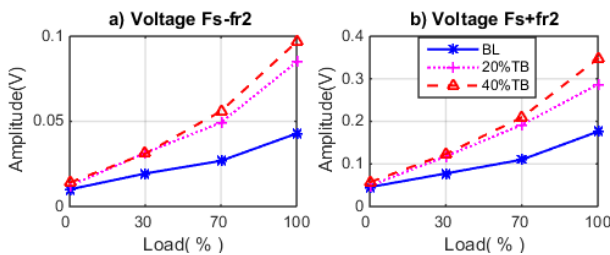


Figure 9. Voltage peaks at the lower and upper sidebands frequency

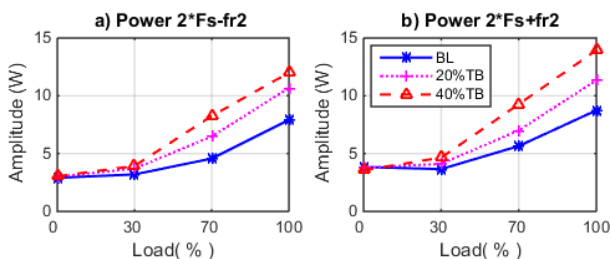


Figure 10. Power peaks at lower and upper sidebands frequency

V. CONCLUSION

In this paper, the effect of a gear tooth breakage on electrical motor signals under sensorless VSD has been studied. Induction motor fault detection was carried out using electrical signature analysis techniques based on a two stage helical gearbox mechanical transmission system driven by a sensorless VSD. It is found that the stator current, voltage and power spectra show an increase in sideband amplitude with load and fault severity under sensorless operating mode. The analysis shows that the spectra produce a noticeable change in the current, voltage and power sideband components. Additionally, the power spectrum gives a slightly larger difference between fault cases. In particular, it provides a consistent change with the fault severity.

REFERENCES

- [1] Viték, O., *Induction machine diagnosis using stator current and magnetic field analysis*. Zeszyty Problemowe–Maszyny Elektryczne, 2009(82).
- [2] Sin, M., W. Soong, and N. Ertugrul. *Induction machine on-line condition monitoring and fault diagnosis–A survey*. in *Australasian Universities Power Engineering Conference*. 2003.
- [3] Mehala, N., *Condition monitoring and fault diagnosis of induction motor using motor current signature analysis*. 2010, NATIONAL INSTITUTE OF TECHNOLOGY KURUKSHETRA, INDIA.
- [4] De Almeida, A., et al., *VSDs for electric motor systems*. Final Report, SAVE Programme, European Commission, Brussels, 2001.
- [5] Abusaad, S., et al. *Utilizing data from a sensorless AC variable speed drive for detecting mechanical misalignments*. in *Key Engineering Materials*. 2013. Trans Tech Publ.
- [6] Rajendra, B.R. and S.V. Bhaskar, *Condition Monitoring of Gear Box by Using Motor Current Signature Analysis*. International Journal of Scientific and Research Publications: p. 563.
- [7] Ashari, D., et al., *Detection and Diagnosis of Broken Rotor Bar Based on the Analysis of Signals from a Variable Speed Drive*. 2014.
- [8] Harnefors, L. and M. Hinkkanen. *Stabilization of sensorless induction motor drives: A survey*. in *2013 IEEE Workshop on Electrical Machines Design, Control and Diagnosis (WEMDCD)*. 2013.
- [9] Carino-Corrales, J.A., et al. *Novel methodology for improving performance of sensorless speed observers in induction motors at variable load conditions*. in *IECON 2012-38th Annual Conference on IEEE Industrial Electronics Society*. 2012. IEEE.
- [10] Abusaad, S., F. Gu, and A. Ball, *Observer-based Fault Detection and Diagnosis for Mechanical Transmission Systems with Sensorless Variable Speed Drives*. 2015.
- [11] Shaeboub, A., et al. *Detection and diagnosis of motor stator faults using electric signals from variable speed drives*. in *Automation and Computing (ICAC), 2015 21st International Conference on*. 2015. IEEE.
- [12] Lane, M., et al., *Investigation of Motor Current Signature Analysis in Detecting Unbalanced Motor Windings of an Induction Motor with Sensorless Vector Control Drive*, in *Vibration Engineering and Technology of Machinery*. 2015, Springer. p. 801-810.
- [13] Haram, M., et al. *An Investigation of the electrical response of a variable speed motor drive for mechanical fault diagnosis*. 2011. COMADEM.
- [14] Alwodai, A., et al. *Modulation signal bispectrum analysis of motor current signals for stator fault diagnosis*. in *Automation and Computing (ICAC), 2012 18th International Conference on*. 2012. IEEE.
- [15] Gutierrez-Villalobos, J.M., et al., *Sensorless FOC Performance Improved with On-Line Speed and Rotor*

- Resistance Estimator Based on an Artificial Neural Network for an Induction Motor Drive*. *Sensors*, 2015. **15**(7): p. 15311-15325.
- [16] Abusaad, S., et al., *Investigating the Effect of Water Contamination on Gearbox Lubrication based upon Motor Control Data from a Sensorless Drive*. 2014.
- [17] Schoen, R.R., et al., *Motor bearing damage detection using stator current monitoring*. *Industry Applications, IEEE Transactions on*, 1995. **31**(6): p. 1274-1279.
- [18] ABB, *Technical Guide No. 100, High Performance Drive-speed and torque regulation, in High Performance Drive-speed and torque regulation*. ABB Industrial Systems, Editor 1996, ABB Industrial Systems, Inc, 1996.
- [19] Gu, F., et al., *Electrical motor current signal analysis using a modified bispectrum for fault diagnosis of downstream mechanical equipment*. *Mechanical Systems and Signal Processing*, 2011. **25**(1): p. 360-372.
- [20] Gu, F., et al. *Motor current signal analysis using a modified bispectrum for machine fault diagnosis*. in *ICCAS-SICE, 2009*. 2009. IEEE.
- [21] Habetler, T.G., *Effects of time-varying loads on rotor fault detection in induction machines*. *Industry Applications, IEEE Transactions on*, 1995. **31**(4): p. 900-906.
- [22] Gu, F., et al., *A new method of accurate broken rotor bar diagnosis based on modulation signal bispectrum analysis of motor current signals*. *Mechanical Systems and Signal Processing*, 2015. **50**: p. 400-413.